J Nanopart Res (2024) 26:111
https://doi.org/10.1007/s11051-024-06020-4

RESEARCH

One-order closed model of fluctuating particle coagulation term in the Reynolds averaged general dynamic equation for nanoparticles

Wenqian Lin · Hailin Yang · Jianzhong Lin

Received: 22 December 2023 / Accepted: 13 May 2024 / Published online: 20 May 2024

Abstract The effect of fluctuating coagulation on particle distribution in multiphase turbulence of nanoparticles was studied based on the Reynolds averaged equation of turbulence flow and the general dynamic equation of particles. A one-order closed model was proposed to relate the fluctuating coagulation term to the average particle size distribution function for closing the particle equation. The proposed model and equations were applied to a turbulent jet flow using the *k*-*ε* turbulent model and the Taylor-series expansion moment method. The results showed that there is a difference in the values of particle number density M_0, geometric average diameter d_{pg} and geometric standard deviation σ_g of particle diameter with and without considering fluctuating coagulation. Larger Damkohler number leads to smaller M_0, higher particle polydispersity M_2, larger d_{pg} and σ_g. Along the x direction of the flow, M_0 decreases, while M_2, d_{pg} and σ_g increase. From the centerline to the outer edge of the jet, M_0, M_2 and d_{pg} decrease, while σ_g increases first and then decreases. Finally, the further research that can be carried out has been proposed.

Keywords Nanoparticles · Fluctuating coagulation · One-order closed model · Particle distribution · Turbulent jet flow · Numerical simulation

W. Lin
School of Media and Design, Hangzhou Dianzi University, Hangzhou 310018, China

H. Yang · J. Lin (✉)
State Key Laboratory of Fluid Power and Mechatronic Systems, Zhejiang University, Hangzhou 310027, China
e-mail: mecjzlin@public.zju.edu.cn

J. Lin
Zhejiang Provincial Engineering Research Center for the Safety of Pressure Vessel and Pipeline, Ningbo University, Ningbo 315201, China

Introduction

The motion of fluids containing nanoparticles is common in nature and engineering processes, e.g., synthesis of nanostructured materials, drag reduction, improving heat conduction, atmospheric processes and so on. The spatial and temporal evolution of particle number density (PND) and size distribution (PSD) in the flow is governed by the general dynamic equation (GDE) which includes the processes of particle convection and diffusion as well as nucleation, evaporation, condensation, coagulation, breakage and so on [1]. In the GDE, the above processes determine the change in the size distribution function with time and position. By solving the GDE for different initial and boundary conditions, the size distribution function can be calculated for geometries and flow conditions of practical interest.

Among the above process, one of the most typical and common phenomena is particle coagulation which is a process whereby particles collide with one another and adhere to form large particles, resulting in the particle size increased and number density decreased [1]. The particle number density in multiphase flow of nanoparticles is usually high, e.g., cloud formation and synthesis of nanoparticle material structure, which makes particle coagulation the main controlling factor of the GDE. In addition to coagulation, nanoparticles ($10^{-9} \sim 10^{-7}$m) undergo Brownian motion due to the collision of gas molecules, and also exhibit convection and diffusion under the effect of fluid velocity and velocity gradient. Therefore, the main aim of this study is to study the evolution of particle distribution under the combined effect of particle convection, diffusion and coagulation.

In most applications, the flow of fluids containing nanoparticles is in turbulent state. In this case, turbulence not only affects particle convection and diffusion, but also affects particle coagulation. The nonlinear interaction between turbulence and particle coagulation makes the problem very complex. One of the factors leading to particle coagulation is particle collision which is affected by the turbulence. Some investigations have been performed to explore the effect of turbulence on the particle collision. Saffman & Turner [2] presented expressions for the turbulent coagulation kernel and applied the expressions to show how the size distribution of particle will change by numerical integration. Delichatsios & Probstein [3] derived coagulation rate relations for particle sizes less than and larger than the Kolmogorov microscale of turbulence, and indicated that the coagulation efficiency did not depend on the particle transport mode. Sundaram & Collins [4] indicated that collision rates of particles that rebound elastically were controlled by the statistics of radial distribution of particles and the relative velocity probability density function. Wang et al. [5] argued through numerical experiments that the expressions presented by Saffman & Turner [2] were correct only when the particles were kept in the system after collision and allowed to overlap in space. Reade & Collins [6] found that the formula derived by Sundaram & Collins [4] was equally valid in a coagulating system, and indicated that coagulation altered the numerical values of statistics from the values they attained for the elastic rebound case. Guichard et al. [7] revealed the necessity to consider the Brownian motion and turbulence effects together in the coagulation kernel. Finke et al. [8] found the elevation of droplet collision frequency when applying the multiple orifices to reduce the droplet coagulation due to the establishment of a turbulent mixing zone. Chen and Cheng [9] showed that the Nusselt number was increased with increasing nanoparticle concentrations because the probability of collision of particles was increased in the cooling stave of blast furnace. Karsch and Kronenburg [10] incorporated an interpolation scheme to extend the expression of coagulation kernel which was originally developed for the ballistic and diffusive agglomeration to the more general transition regime. In addition, the surface properties of particles also have an impact on particle collisions, e.g., like-charged conducting particles almost always attract each other at small separations [11]; the enhancement factor of collision rate was dependent only on the Stokes number, the electrostatic energy to shear energy ratio, and the ratio of colliding particle radii for particles of constant surface charge density [12].

The effect of turbulence on particle coagulation after collision is another important research topic and is also the focus of this article. For obtaining the PSD and PND by solving the GDE, the effect of turbulence on particle coagulation is specifically the effect of turbulence fluctuation on the PSD and PND. There have been some studies in this topic. Levin & Sedunov [13] studied the gravitational coagulation of charged cloud drops in turbulent flow with respect to the electrostatic forces. Soos et al. [14] built a micromixing model by assuming a probability density function (PDF) to represent the interaction between fluctuations and particle coagulation in turbulent jets. Guichard et al. [7] indicated that it was necessary to consider the Brownian and turbulence effects together in the coagulation kernel. Cifuentes et al. [15] studied the effect of turbulence on particle-forming flames and captured a number of the Batchelor scales pertaining to the smaller nanoparticle structures. The physical mechanisms that contribute to particle growth were not negligible on the particle concentrations. Anand and Mayya [16] showed that the spatial inhomogeneity in the particle number concentration initiated differential coagulation rates leading to a distribution with larger size modes in regions with higher concentration, and sharper the occurrence of spatial heterogeneity, more pronounced was the bimodal effect. Papini et al. [17] obtained a precise link between mean intensity of the turbulent velocity field and coagulation enhancement, and proved a formula for the mean velocity difference, in agreement with the gas-kinetic model by a new method. Zhao et al. [18] found that the coagulation of particles less than 130 nm was dominated by Brownian motion, while turbulent coagulation significantly affected the coagulation of particles with diameters of 600–950 nm in vehicle plumes. Zatevakhin et al. [19] considered Brownian coagulation under turbulent mixing conditions, and demonstrated that the use of Reynolds-averaged equations could lead to a significant underestimation of coagulation rates. Chan et al. [20] investigated nanoparticle formation, coagulation and condensation processes in turbulent flows, and showed that the large coherent structures strongly affected the particle number and mass concentration distributions as well as particle polydispersity.

The particle coagulation term in the GDE for turbulent flow can also be solved using direct numerical simulation (DNS), large eddy simulation (LES), and Reynolds averaged method (RAM). In terms of solving the GDE by the DNS and LES, Settumba & Garrick [21] defined a Damköhler number to represent the ratio of the convection to coagulation time scales, and obtained the evolution of the particle field using a moment method to approximate the GDE. Miller & Garrick [22] performed the DNS of nanoparticle coagulation in a planar jet using a sectional method to approximate the GDE without a priori assumptions regarding the particle size distribution. Garrick et al. [23] conducted the DNS of a coagulating aerosol in a 2-D iso-thermal shear layer utilizing a nodal model to approximate the GDE with no a priori assumptions of the particle size distribution at $Re=200$. Garrick [24] used the data of direct numerical simulation to isolate the impact of small or subgrid-scale particle–particle interactions on particle coagulation, and showed that small-scale interactions acted to both promote and suppress particle coagulation. Ma et al. [25] implemented a coupling of the DNS and the GDE to explore the impact of turbulence on nanoparticle dynamics in homogenous isotropic turbulence using the Taylor-series expansion method of moments, and indicated that the coagulation had a significant effect on the particle dynamics. Cifuentes et al. [26] introduced a new DNS database to obtain insights into the statistics of nanoparticle formation in reactive flows using the sectional method to solve the GDE. Schwarzer et al. [27] applied the DNS with a Lagrangian particle tracking strategy in combination with the coupled population balance-micromixing approach, and found that the approach was capable of predicting not only the mean sizes but the full PSD. Das & Garrick [28] calculated instantaneous, filtered and spanwise averaged data of the particle field in a planar turbulent jet via DNS for examining the turbulent fluctuations on particle growth, and indicated that turbulence or subgrid scale models were needed for accurately simulating particle dynamics.

The DNS does not require establishing a model for turbulence and directly solving the Navier–Stokes equation numerically, which can avoid modeling errors. However, turbulence is a multi-scale irregular flow. To obtain flow information at all scales, there is a high demand for spatial and temporal resolution. Using the DNS requires a large amount of computation, and is highly dependent on computer memory. Therefore, the RAM, i.e., decomposing the particle concentration field into time-averaged and fluctuations has become an alternative method. Rigopoulos [29] applied Reynolds averaging (i.e., decomposing fluid velocity and particle size distribution function into time-averaged and fluctuations) to the GDE and obtained Reynolds averaged GDE (RA-GDE). In the RA-GDE, the coagulation birth and death terms include second-order correlation of two fluctuating particle size distribution function, the correlation is the contribution to coagulation resulting from the fluctuating concentrations hence it is called fluctuating coagulation term (FCT). The presence of the FCT makes the RA-GDE unclosed, so the FCT is usually assumed to be negligible (e.g., [30–32]) or other methods are used to avoid the closed problem of the equation. For example, Rigopoulos [29] proposed a new probability density function (PDF) method based on the transport of the joint PDF of reactive scalars and the PND at different sizes to overcome the closure problems, and indicated that the interaction of turbulence with particle formation mechanisms accounted for significant deviations in the PSD in some cases and could not be neglected. Tsagkaridis et al. [33] used sectional method for the GDE coupled with the DNS for the flow equation to investigate turbulence-coagulation interaction in a 3-D turbulent planar jet, and the FCT was simulated via the DNS. The results showed that the FCT made a significant contribution to the time-averaged coagulation term, up to 20% on the jet centreline and 40% close to the edges.

The FCT cannot be ignored in some cases beads on the preceding review. There have been similar views in the past [1, 34]. In addition to the above methods for handling the FCT to avoid the problem of equation closure, the method of directly modeling the FCT to close the equation is an alternative method. Inspired by the fact that Reynolds stress (second-order correlations of two fluctuating velocity) is expressed as the product of eddy viscosity coefficient and average velocity, the FCT (second-order correlations of two fluctuating particle size distribution function) can be expressed as the product of a coefficient of turbulent fluctuation and average particle size distribution function, thus closing the equation. Similar to turbulence model, if a differential equation needs to be solved when determining the coefficient of turbulent fluctuation, this mode is called a one-order closed mode. Previous studies have directly used kinetic energy and turbulent kinetic energy to represent the coefficient of turbulent fluctuation, while the innovation of this article is to obtain this coefficient through a more accurate method of solving the equation of fluctuating particle concentration. Therefore, This paper aims to develop a one-order closed model in which the equation of fluctuating particle concentration is involved, and apply the model to solve RA-GDE in a turbulent jet flow to demonstrate the necessity of retaining the FCT (i.e., involving turbulence– coagulation interaction).

The rest of this paper is structured as follows. Section II presents the basic equations including the closed process of the RA-GDE. In Section III, the moment equation of particles and Taylor-series expansion moment method are introduced. Subsequently, the model, equations are applied to a turbulent jet flow in Section IV where details on the flow configuration, numerical parameters and method, verification and discussion of numerical result are presented. Finally, the conclusions are presented in section V.

Basic equations

In the present study the following assumptions are made: (1) The concentration of particles is not high enough to change the constitutive relationship of the fluid, and the fluid remains a Newtonian fluid. In addition, the particles do not affect the fluid density and viscosity, and in gas-particle two-phase flow, if the volume concentration of particles is less than 10^{-6} (the concentration in this paper is 1.79×10^{-7} as shown in IV B), the particle phase is called dilute phase and the one-coupling model (the particles have no impact on the fluid motion) can be used. (2) The ratio of the response time scale of the particles to the characteristic time scale of flow (i.e., Stokes number) is much smaller than unity so that the particles follow the fluid. (3) The particles are spherical before coagulation, and coagulated particles are modelled by a spherical particle with the equivalent volume. Above assumptions can be found in realistic applications.

Flow field

The flow is considered as incompressible and isothermal. The instantaneous velocity and pressure can be written as the sum of average and fluctuating components based on the method of Reynolds average:

$$u_i = \overline{u}_i + u'_i,\ p = \overline{p} + p' \ . \tag{1}$$

Substituting Eq. 1 into the continuity and Navier Stokes equation and averaging with respect to time, we have

$$\frac{\partial \overline{u}_i}{\partial x_i} = 0, \tag{2}$$

$$\frac{\partial \overline{u}_i}{\partial t} + \overline{u}_j \frac{\partial \overline{u}_i}{\partial x_j} = -\frac{1}{\rho}\frac{\partial \overline{p}}{\partial x_i} + \frac{\mu}{\rho}\frac{\partial^2 \overline{u}_i}{\rho \partial x_i \partial x_i} - \frac{\partial \overline{u'_i u'_j}}{\partial x_j}, \tag{3}$$

in which $\overline{u}_i$ and $\overline{p}$ are the average fluid velocity and pressure, ρ and μ are the fluid density and viscosity, respectively; $-\rho\overline{u'_i u'_j}$ is the Reynolds stress and related to the gradient of average velocity based on the turbulent viscosity hypothesis:

$$-\rho\overline{u'_i u'_j} + \frac{2}{3}\rho k \delta_{ij} = 2\mu_t \left(\frac{\partial \overline{u}_i}{\partial x_j} + \frac{\partial \overline{u}_j}{\partial x_i} \right), \tag{4}$$

$$k = \frac{1}{2}\overline{u'_i u'_i},\ \mu_t = C_\mu \frac{\rho k^2}{\varepsilon}, \tag{5}$$

where μ_t is the eddy viscosity; C_μ is a constant and taken as 0.09 here; k and ε are the turbulent kinetic energy and turbulent dissipation rate, respectively, and can be described as:

$$\rho\overline{u}_j\frac{\partial k}{\partial x_j} = -\rho\overline{u'_i u'_j}\frac{\partial \overline{u}_i}{\partial x_j} - \rho\varepsilon + \frac{\partial}{\partial x_j}\left[\left(\mu + \frac{\mu_t}{\sigma_k}\right)\frac{\partial k}{\partial x_j}\right], \tag{6}$$

$$\rho\overline{u}_j\frac{\partial \varepsilon}{\partial x_j} = -C_1\frac{\varepsilon}{k}\rho\overline{u'_i u'_j}\frac{\partial \overline{u}_i}{\partial x_j} - C_2\rho\frac{\varepsilon^2}{k} + \frac{\partial}{\partial x_j}\left[\left(\mu + \frac{\mu_t}{\sigma_\varepsilon}\right)\frac{\partial \varepsilon}{\partial x_j}\right], \tag{7}$$

where the constants are taken as $C_1 = 1.44$, $C_2 = 1.92$, $\sigma_k = 1.0$ and $\sigma_\varepsilon = 1.3$.

Particle field

The instantaneous particle size distribution function $n(v, t)$ (v is particle volume) also can be decomposed into average and fluctuating components:

$$n = \overline{n} + n'. \tag{8}$$

The motion of particle is related to the particle drag. In this paper, a dual fluid model is used, and the drag exerted by the fluid on the particles is reflected in the particle convection and diffusion terms of Eq. 9. Substituting Eqs.8 and 1 into the general dynamic equation (GDE) for nanoparticles and averaging with respect to time yields:

$$\begin{aligned}\frac{\partial \overline{n}(v,t)}{\partial t} + \overline{u}\cdot\nabla\overline{n}(v,t) - \nabla\cdot[D_p\nabla\overline{n}(v,t)] + \nabla\cdot\overline{n'u'} &= \frac{1}{2}\int_0^v \beta(v_1, v-v_1)\overline{n}(v_1,t)\overline{n}(v-v_1,t)\mathrm{d}v_1 \\ &- \int_0^\infty \beta(v_1,v)\overline{n}(v,t)\overline{n}(v_1,t)dv_1 \\ &+ \frac{1}{2}\int_0^v \beta(v_1, v-v_1)\,\overline{n'(v_1,t)n'(v-v_1,t)}\,\mathrm{d}v_1 \\ &- \int_0^\infty \beta(v_1,v)\,\overline{n'(v,t)n'(v_1,t)}\,\mathrm{d}v_1\end{aligned}, \tag{9}$$

on the left-hand side, the first, second, third, fourth term are the unsteady, convection, diffusion and turbulent diffusion term, respectively. On the right-hand side, the first and third terms are the birth, and the second and fourth terms are the death of particles due to coagulation, respectively;$\overline{u}$ and $\boldsymbol{u'}$ are the average and fluctuating velocity vector; D_p is the particle diffusion coefficient. For nanoparticles, D_p needs to be corrected based on the Cunningham slip correction coefficient C_c [1]:

$$D_p = \frac{k_b T C_c}{3\pi\mu d_p}, = 1 + Kn[1.257 + 0.40\exp(\frac{-1.10}{Kn})], \tag{10}$$

in which k_b is the Boltzmann constant; T is the temperature; d_p is the particle diameter; $Kn = 2\lambda/d_p$ is the Knudsen number with λ being the mean free path of gas molecules. Interpolation formula 10 is often used to cover the entire range of values of the Knudsen number from the continuum to the free molecule regimes.

In Eq. 9 $\beta(v, v_1)$ is the coagulation kernel for two particles with volume of v and v_1, and describes the frequency of collisions leading to coagulation. The particle coagulation is mainly induced by Brownian motion, laminar and turbulent shear. When the particle size is less than 1 μm and the particle concentration is less than the critical value corresponding to turbulent coagulation, the particle coagulation is mainly dominated by the Brownian motion, so the Brownian coagulation kernel in the free molecular region is:

$$\beta(v, v_1) = (\frac{3}{4\pi})^{1/6}(\frac{6k_b T}{\rho_p})^{1/2}(v^{1/3} + v_1^{1/3})^2, \tag{11}$$

where ρ_p is the particle density. The initial diameter of the particles is on the nanoscale, and the ratio of the diameter after coagulation to the initial diameter is less than 7 times as shown in Fig. 10. Therefore, the diameter of the particles after coagulation is still less than or equal to the molecular free path, so Eq. 11 can still be used.

The last term on the left-hand side of Eq. 9 represents the change in $\overline{n}$ resulting from turbulent diffusion. The term can be treated in a manner similar to passive scalar advection based on the assumption that particles are small and of zero inertia [1]:

$$\overline{n' u_i'} = -\frac{\mu_t}{\rho}\frac{\partial \overline{n}}{\partial x_i}, \tag{12}$$

where μ_t is the eddy diffusivity as shown in Eq. 5.

The closure of the GDE and the transport equation of particle concentration fluctuation

The third and fourth term on the right-hand side of Eq. 9, called fluctuating coagulation term (FCT), make the GDE unclosed. The FCT is the contribution to coagulation resulting from the fluctuating concentration. As described in the introduction, the FCT has been neglected in many previous studies, while the FCT holds a certain weight in some practical situations. In the present study, the FCT is treated in a manner similar to Reynolds stress and expressed as the product of a coefficient of turbulent fluctuation ς_t and average particle size distribution function:

$$\overline{n'(v_1,t)n'(v-v_1,t)}=\varsigma_t\overline{n}(v_1,t)\overline{n}(v-v_1,t), \tag{13}$$

$$\overline{n'(v,t)n'(v_1,t)}=\varsigma_t\overline{n}(v,t)\overline{n}(v_1,t). \tag{14}$$

Next we define ς_t as:

$$\varsigma_t=\frac{\overline{(C'_m)^2}}{\overline{(C'_m)^2}+\overline{C}_m{}^2}, \tag{15}$$

where the instantaneous particle concentration C_m is decomposed into average component $\overline{C}_m$ and fluctuating component C'_m, then $\overline{(C'_m)^2}$ is the average value of the square of the fluctuating component C'_m. In Eq. 15 $\overline{(C'_m)^2}$ should be calculated through solving the equation of particle fluctuating concentration, so the model based on Eq. 15 is called one-order closed model.

In a manner similar to turbulent generation and dissipation, during transportation of particles, the generation and dissipation terms of $\overline{(C'_m)^2}$ are:

$$\text{generation} \sim k^{1/2}l(\nabla C_m)^2,\ \text{dissipation} \sim \frac{k^{1/2}}{l}\overline{(C'_m)^2}, \tag{16}$$

where l is the Kolmogorov scale and proportional to $k^{3/2}/\varepsilon$ based on the turbulent $k\sim\varepsilon$ model. The equation of particle fluctuating concentration suitable to the turbulent $k\sim\varepsilon$ model is [35, 36]:

$$\frac{\partial\overline{(C'_m)^2}}{\partial t}+\overline{u}\cdot\nabla\overline{(C'_m)^2}-\nabla\cdot[(\frac{\mu}{\rho}+\frac{\mu_t}{\rho Pr})\nabla\overline{(C'_m)^2}]=C_{g1}\frac{k^2}{\varepsilon}|\nabla C_m|^2-C_{g2}\frac{\varepsilon}{k}\overline{(C'_m)^2}, \tag{17}$$

in which Pr is the Prandtl number of $\overline{(C'_m)^2}$; C_{g1} and C_{g2} are the coefficient and taken as 0.41 and 1.4 [37], respectively.

Closed GDE

Substituting Eqs.12, 13, 15 into Eq. 9, we have:

$$\begin{aligned}\frac{\partial\overline{n}(v,t)}{\partial t}+\overline{u}\cdot\nabla\overline{n}(v,t)-\nabla\cdot[(D_p+\frac{\mu_t}{\rho})\nabla\overline{n}(v,t)]=&\frac{1}{2}\int_0^v\beta(v_1,v-v_1)(1+\frac{\overline{(C'_m)^2}}{\overline{(C'_m)^2}+\overline{C}_m{}^2})\overline{n}(v_1,t)\overline{n}(v-v_1,t)\mathrm{d}v_1\\&-\int_0^\infty\beta(v_1,v)(1+\frac{\overline{(C'_m)^2}}{\overline{(C'_m)^2}+\overline{C}_m{}^2})\overline{n}(v,t)\overline{n}(v_1,t)dv_1\end{aligned}, \tag{18}$$

where D and β are shown in Eqs. 10 and 11, respectively. Equation 18 is the closed general dynamic equation (GDE).

Moment equation and moment method

Moment equation

The numerical method should be used to solve the closed GDE because of the complexity of the equation. In the numerical methods including the DNS, moment method, sectional method and stochastic particle method, the moment method has been widely utilized due to its relative simplicity of the calculation and the need for relatively few computing resources. In the moment method, the moment of average particle size distribution function is defined by:

$$m_k=\int_0^\infty v^k\overline{n}(v)dv, \tag{19}$$

where k is the order of the moment; the zero-order moment m_0 represents the total number density of particles at given point and time; the first-order moment m_1 is the total volume concentration of particles; the second-order moment m_2 is proportional to the particle polydispersity; and the higher-order moments with $k>2$ represent different physical meanings.

Before using the moment method, it is necessary to transform the GDE into a moment equation. Based on Eq. 19, the GDE is transformed into the moment equation after multiplying Eq. 18 by v^k and then integrating over the entire size distribution:

$$\frac{\partial m_k}{\partial t}+\overline{u}\cdot\nabla m_k-\nabla\cdot[(D_p+\frac{\mu_t}{\rho})\nabla m_k] = \frac{1}{2}\int_0^\infty\int_0^\infty[(v+v_1)^k-v^k-v_1^k](1+\frac{(\overline{C_m\prime})^2}{(C_m\prime)^2+\overline{C}_m{}^2}) \beta(v,v_1)\overline{n}(v,t)\overline{n}(v_1,t)\mathrm{d}v\mathrm{d}v_1. \tag{20}$$

Equation 20 is the moment equation for nanoparticles in turbulent flow.

Taylor-series expansion moment method

The moment equation has been solved using different moment methods in the past, e.g., pre-assuming the shape of particle size distribution [38], approximating the integral moment through an n-point Gaussian quadrature [39], approximating moments to pth-order polynomials [40], closuring equation with interpolative method [41], and closuring equation with the Taylor-series expansion [42]. The last moment method, called the Taylor-series expansion moment method (TEMOM), has been effectively applied in the past [43–46] and hence adopted in the present study. The TEMOM is expanding the coagulation kernel of particles with particle volume as a small parameter using Taylor series to make it an integrable function and make the moment equation solvable in a closed form. For a detailed introduction to the TEMOM is referred to [42].

Substituting Eq. 11 into Eq. 20 with $k=0$, 1, 2, we have:

$$\frac{\partial m_0}{\partial t}+\overline{u}\cdot\nabla m_0-\nabla\cdot[(D_p+\frac{\mu_t}{\rho})\nabla m_0] = -(\frac{3}{4\pi})^{1/6}(\frac{6k_bT}{\rho_p})^{1/2}(1+\frac{(\overline{C_m'})^2}{(C_m')^2+\overline{C}_m{}^2})(m_0m_1+3m_{1/3}m_{2/3}), \tag{21a}$$

$$\frac{\partial m_1}{\partial t}+\overline{u}\cdot\nabla m_1-\nabla\cdot[(D_p+\frac{\mu_t}{\rho})\nabla m_1]=0, \tag{21b}$$

$$\frac{\partial m_2}{\partial t}+\overline{u}\cdot\nabla m_2-\nabla\cdot[(D_p+\frac{\mu_t}{\rho})\nabla m_2] = (\frac{3}{4\pi})^{1/6}(\frac{6k_bT}{\rho_p})^{1/2}(1+\frac{(\overline{C_m\prime})^2}{(C_m\prime)^2+\overline{C}_m{}^2}) (m_1m_2+3m_{4/3}m_{5/3}), \tag{21c}$$

where integer and fractional order moments are included. For closing Eq. 21, the TEMOM is used to expand v^k at point $v=w$ and remain the first three term of Taylor series. Thus v^k can be transformed into:

$$v^k=(\frac{w^{k-2}k^2}{2}-\frac{w^{k-2}k}{2})v^2 +(-w^{k-1}k^2+2w^{k-1}k)v+w^k +\frac{w^kk^2}{2}-\frac{3w^kk}{2}. \tag{22}$$

Combining Eq. 22 with Eq. 19 yields:

$$m_k=(\frac{v^{k-2}k^2}{2}-\frac{v^{k-2}k}{2})m_2+(-v^{k-1}k^2 +2v^{k-1}k)m_1+(v^k+\frac{v^kk^2}{2}-\frac{3v^kk}{2})m_0. \tag{23}$$

Substituting Eq. 23 into Eq. 21, we have:

$$\frac{\partial m_0}{\partial t}+\overline{u}\cdot\nabla m_0-\nabla\cdot[(D_p+\frac{\mu_t}{\rho})\nabla m_0] = -\frac{\sqrt{2}}{5184}(\frac{3}{4\pi})^{1/6}(\frac{6k_bT}{\rho_p})^{1/2}(1+\frac{(\overline{C_m\prime})^2}{(C_m\prime)^2+\overline{C}_m{}^2}) \frac{m_0^{11/6}(-65m_0^2m_2^2+1210m_0m_1^2m_2+9223m_1^4)}{m_1^{23/6}} \tag{24a}$$

$$\frac{\partial m_1}{\partial t}+\overline{u}\cdot\nabla m_1-\nabla\cdot[(D_p+\frac{\mu_t}{\rho})\nabla m_1]=0, \tag{24b}$$

$$\frac{\partial m_2}{\partial t}+\overline{u}\cdot\nabla m_2-\nabla\cdot[(D_p+\frac{\mu_t}{\rho})\nabla m_2] = \frac{\sqrt{2}}{2592}(\frac{3}{4\pi})^{1/6}(\frac{6k_bT}{\rho_p})^{1/2}(1+\frac{(\overline{C_m\prime})^2}{(C_m\prime)^2+\overline{C}_m{}^2}) (\frac{-70m_0^2m_2^2+4210m_0m_1^2m_2+6859m_1^4}{m_0^{1/6}m_1^{11/6}}). \tag{24c}$$

Equations 3, 6, 7, 17, 24 form a group of closed equations, and by solving this group of equations, information on flow motion and particle distribution can be obtained.

Application to a turbulent jet flow

In order to validate the availability of the model and equations, we apply Eqs. 3, 6, 7, 17, 24 to a turbulent jet flow.

Flow field

The motion of fluids containing nanoparticles in a turbulent jet is shown in Fig. 1 where the width of the slot is D, the computational domain with $60D \times 41D$ is discretized into a structured grid.

Boundary condition and initial condition

The top-hat profile of average velocity U_{in} at the jet inlet is [47]:

$$U_{\text{in}} = \frac{U_J + U_\infty}{2} + \frac{U_J - U_\infty}{2}\tanh\left(\frac{-|y| + D/2}{2\theta_m}\right), \quad (25)$$

where U_J and U_∞ are the the maximum velocity at the jet inlet and velocity of background flow, respectively. The velocity of background flow is a small non-zero value $U_\infty = 0.2U_j$. $\theta_m = D/20$ is the momentum thickness of shear layer [48].

The moments m_0, m_1 and m_2 at the jet inlet also follow the distribution of top-hat profile. At the exit of the jet, the velocity and moments satisfy the non reflective boundary conditions.

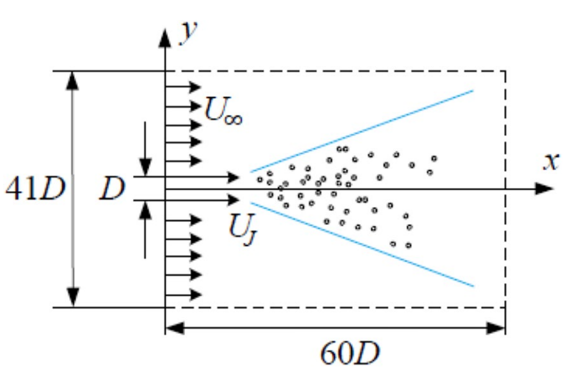

Fig. 1 Jet flow and the coordinate system

The initial maximum vales of m_0, m_1 and m_2 are $m_{00\max} = 2.73 \times 10^{18}$, $m_{10\max} = 1.79 \times 10^{-7}$, $m_{20\max} = 1.17 \times 10^{-32}$, respectively, to make the Damkohler number as shown in expression 26 be unity, thus the effect of convective and coagulation are well coupled [38]. The second subscript 0 of m represents the initial value. The units of $m_{00\max}$, $m_{10\max}$ and $m_{20\max}$ are m^{-3}, 1 and m^3, respectively. The particle is monodisperse at the inlet, thus the polydispersity index $m_{00}m_{20}/m_{10}{}^2 = 1$ [38].

Parameters

The Reynolds number of the flow is defined as $Re = U_J D\rho/\mu$, and the Damkohler number is the ratio of the convective time scale τ_{con} to the coagulation time scale τ_{coa}:

$$Da = \frac{\tau_{\text{con}}}{\tau_{\text{coa}}} = \frac{D/U_J}{(AN_0 v_0{}^{1/6})^{-1}} = \frac{DAN_0 v_0{}^{1/6}}{U_J}, \quad (26)$$

where N_0 is the initial total number density of particles; v_0 is the initial average volume of particles; A is the coagulation coefficient induced by Brownian motion, $A = (3/4\pi)^{1/6}(6k_b T/\rho_p)^{1/2}$. $Da = 0$ indicates that particles do not coagulate because the coagulation time scale is infinity, while $Da \to$ infinity implies that coagulation occurs instantaneously because the coagulation time scale is zero and all particles are instantaneously converted to the largest particle. The main aim of this articles is to illustrate the effect of fluctuating coagulation on particle distribution, so $Da = 1$ and 1/3 are selected in this paper to clarify the effect of fluctuating coagulation on particle distribution when the convection and coagulation effects are equivalent ($Da = 1$) and when convection effect is predominant ($Da = 1/3$) because the larger convection effect leads to a stronger turbulent fluctuating of the flow.

Some parameters are: $\rho = 1.205$ kg/m^3, $\rho_p = 2200$ kg/m^3, $\mu = 1.81 \times 10^{-5}$ Pa•s, $T = 295.15$ K, $k_b = 1.38 \times 10^{-23}$ J/K. The Reynolds number based on the width of the slot D is 3×10^4.

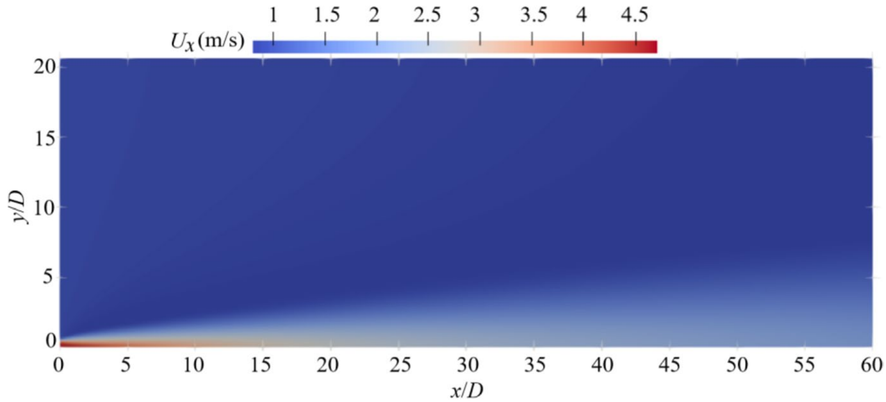

Fig. 2 Average velocity distribution of flow

Numerical method

Equations 3, 6, 7, 17, 24 are solved numerically with the finite volume method in OpenFOAM-5, and the term of velocity–pressure coupling and the convection term are dealt with OpenFOAM SIMPLE algorithm.

A two-dimensional numerical simulation is implemented. Extensive tests and refinements of the independence and suitability of the grid size for the convergence results are performed. The deviations of first three moments M_0, M_1 and M_2 are within 0.01% for the cases of coarse meshes ($560 \times 412 = 230720$ cells) and fine meshes ($810 \times 640 = 518400$ cells), and hence 230720 cells are used in the simulation.

Verification

Rationality of computational domain selection

The distribution of average velocity U_x in the x-direction of the flow is shown in Fig. 2 where only the upper half of the flow is given due to the symmetry of the flow and $D = 0.01$m. Figure 3 shows the distribution of average relative volume concentration ($M_1 = m_1/m_{10}$, $m_{10} = 1.79 \times 10^{-7}$) of particles, and m_{10} is the initial value of m_1. From Figs. 2 and 3 it can be seen that both U_x and M_1 continuously decay along the x and y directions. At $x/D = 60$, the values of U_x and M_1 are 0.912 and 0, respectively, from $y/D = 7.5$ to 20, indicating that the width of the computational domain is sufficient.

Self similarity

The average velocity profile exhibits self similarity along the x direction, which is shown in Fig. 4 where U_c is the velocity on the centerline, and y_h is the half width of the jet, i.e., the y-coordinate corresponding to a point where the flow velocity is half of the centerline velocity at the same x. It can be seen that the velocity profiles at different x positions overlap (self similarity), and numerical results are in good agreement with the experimental results of Gutmark & Wygnanski [49] and Ramaprian & Chandrasekhara [50].

Similar to velocity distribution, a scalar should also satisfy self similarity distribution along the

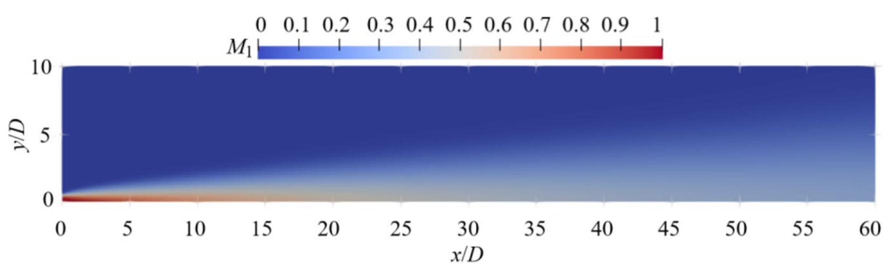

Fig. 3 Distribution of average relative volume concentration of particles

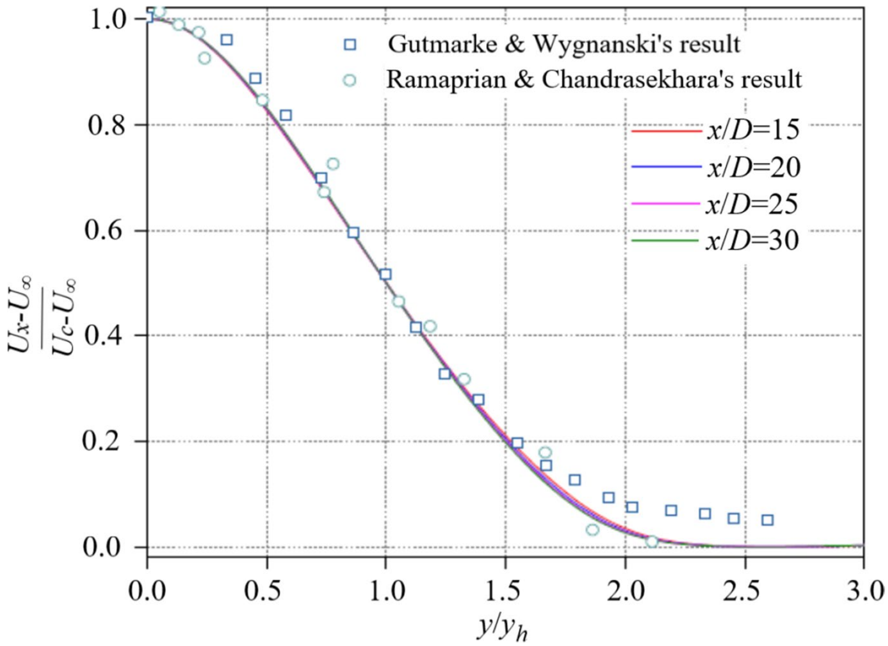

Fig. 4 Self similarity curves of velocity profile on different cross-section

x direction. The variations of m_1/m_{1c} with y/y_h are shown in Fig. 5 where m_{1c} is the value of m_1 on the centerline, and y_h is the y-coordinate corresponding to a point where the value of m_1 is half of the m_1 on the centerline at the same x. It also can be seen that the values of m_1/m_{1c} at different x satisfy self similarity distribution, and numerical results are basically consistent with the experimental results

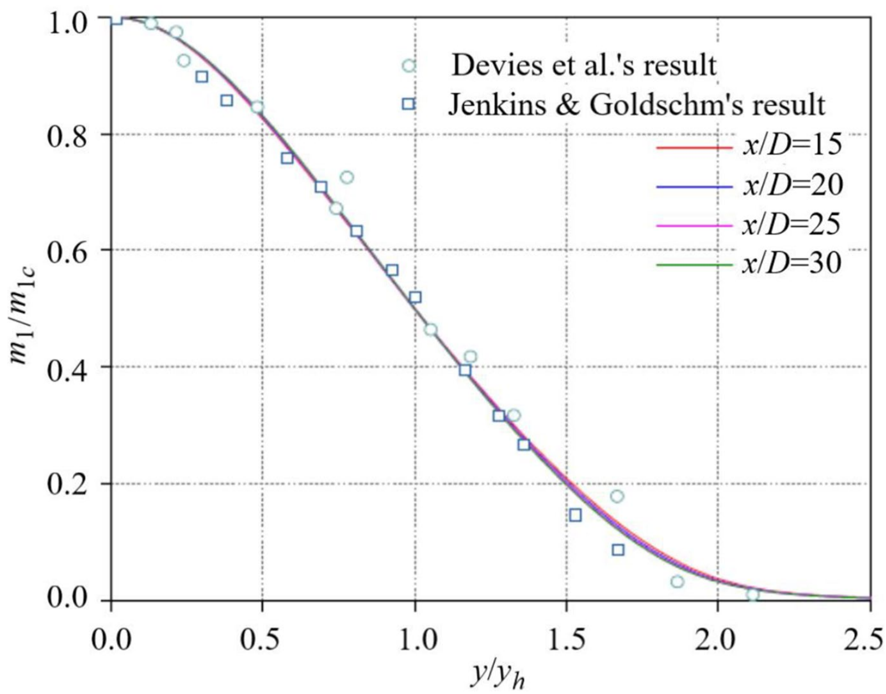

Fig. 5 Distribution of average relative volume concentration of particles

(temperature as a scalar) of Davies et al. [51] and Jenkins & Goldschm [52].

Distribution of x-component of turbulent kinetic energy along the y direction

The distributions of x-component of turbulent kinetic energy along the y direction at different downstream position are shown in Fig. 6 where the experimental result [53] is also given, which shows that both numerical and experimental results are basically consistent.

Result and discussion

Particle number density

The relative number density of particles is expressed as $M_0 = m_0/m_{00}$ (m_{00} is the initial value of m_0). m_0 is described by Eq. 24a where the source term on the right-hand side indicates that particle coagulation will reduce particle number density and therefore take a negative sign. Figure 7 shows the distribution of relative number density of particles at $Da = 1$ and 1/3. We can see that the values of M_0 gradually decrease along the x and y directions. The reason is that, on the one hand, the mixing effect of the jet flow reduces the particle number density M_0, and more importantly, the coagulation effect of the particles greatly reduces M_0. From Eq. 26, the larger the value of Da, the shorter the time scale of particle coagulation, the faster the particle coagulates, and leading to a smaller value for M_0 in the same region, which can be illustrated by comparing Fig. 7(a) and (b) where the values of M_0 are small at $Da = 1$ (a) than that at $Da = 1/3$ (b) in the same region.

Distribution of relative number density M_0 for $Da = 1$ and 1/3 along the x direction is shown in Fig. 8 where the results with considering the fluctuating coagulation (ς_t is represented by Eq. 15) and without considering the fluctuating coagulation ($\varsigma_t = 0$) are compared. The values of M_0 decrease continuously downstream due to particle coagulation. The larger the value of Da, the faster the particle coagulates, and the smaller values of M_0. The value of M_0 for $Da = 1/3$ is 2.77 times that for $Da = 1$ at $x/D = 25$, but 3.67 times at $x/D = 60$. It can be seen that the further downstream, the greater the difference in values of M_0 between for $Da = 1/3$ and for $Da = 1$. In the area near the jet inlet ($x/D < 10$), the

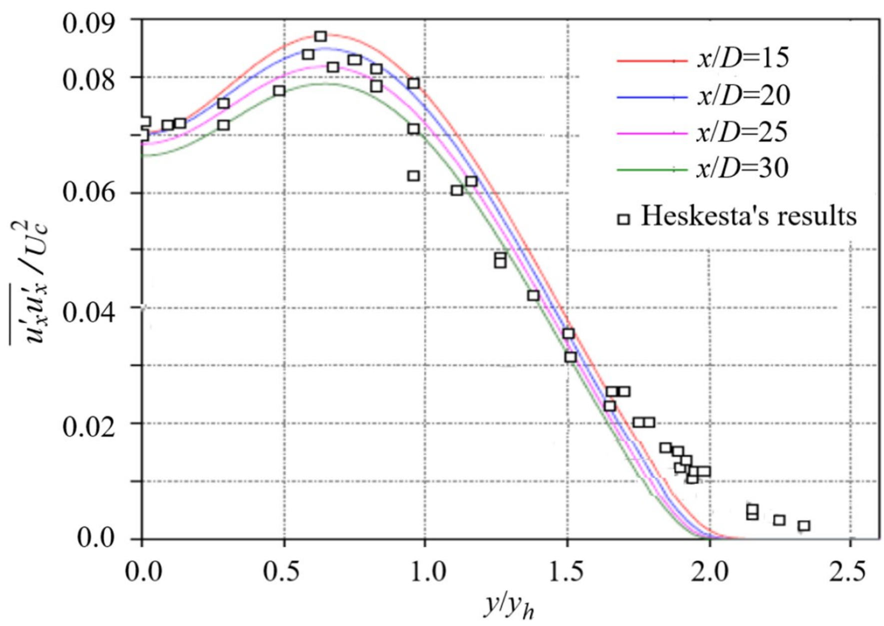

Fig. 6 Distribution of x-component of turbulent kinetic energy along the y direction

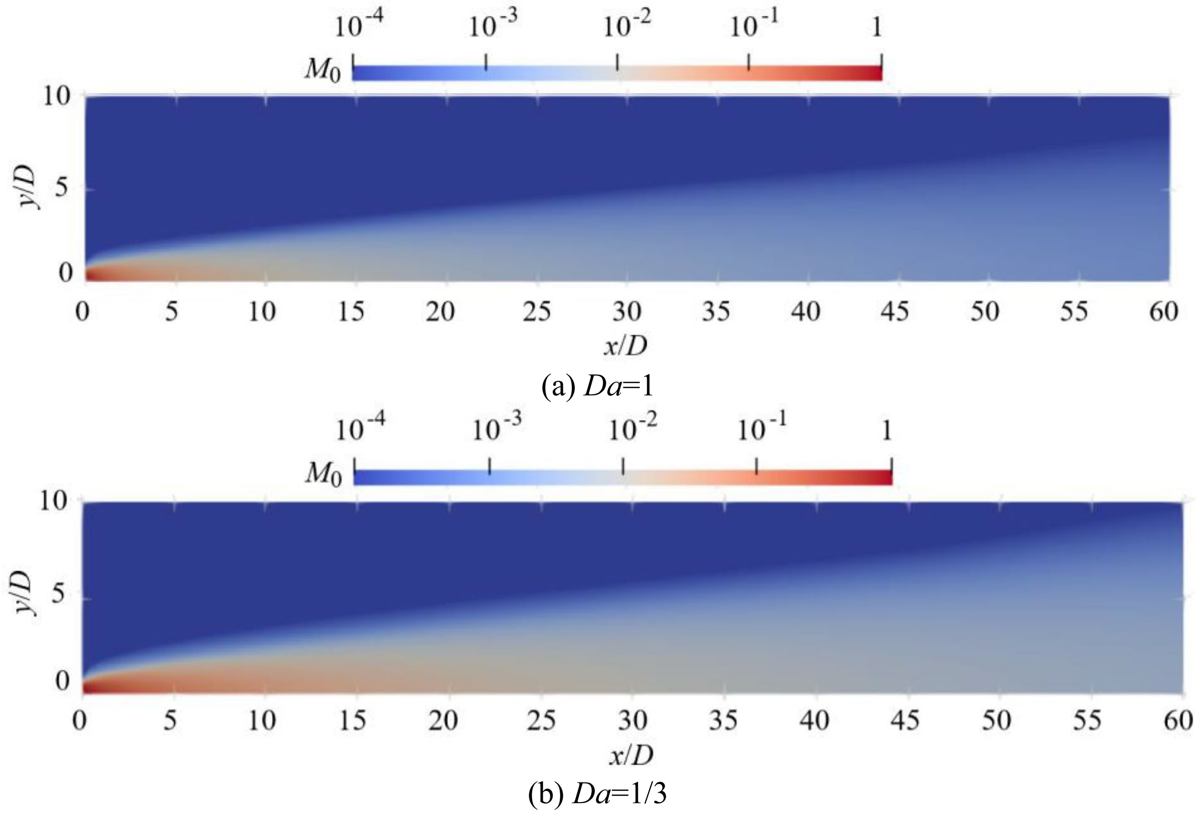

Fig. 7 Distribution of relative number density of particles. (**a**) $Da = 1$. (**b**) $Da = 1/3$

values of M_0 with considering and without considering the fluctuating coagulation are almost the same because the effect of particle coagulation is

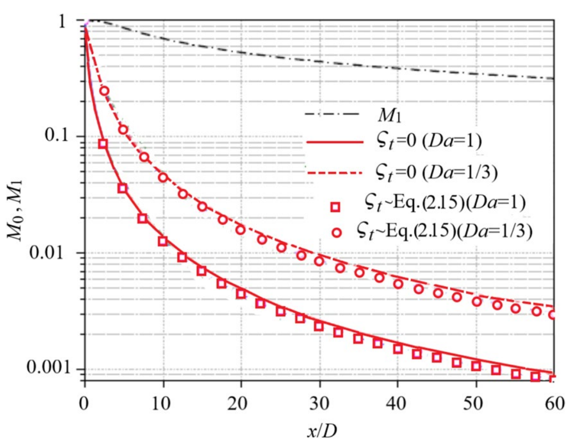

Fig. 8 Distribution of relative number density M_0 and volume concentration M_1 along the x direction

insignificant in this area, however, the differences in the values of M_0 between both cases gradually increases along the downstream. The maximum relative errors (at $x/D = 60$) reach 10.7% for $Da = 1/3$and 17.5% for $Da = 1$, respectively.

Particle coagulation will change the particle number density, but it will not change the particle volume concentration m_1, as shown in Eq. 24b describing m_1, this equation is not related to coagulation. Figure 8 also shows the distribution of relative volume concentration M_1 on the centerline along the x direction. The values of M_1 on the centerline decrease slightly along the downstream, indicating that particles on the centerline gradually diffuse towards both sides. The value of M_1 is much greater than that of M_0 because the particle coagulation does not affect the value of M_1. However, particle coagulation will change the volume of the coagulated particle and further affect the particle volume distribution in computational cells.

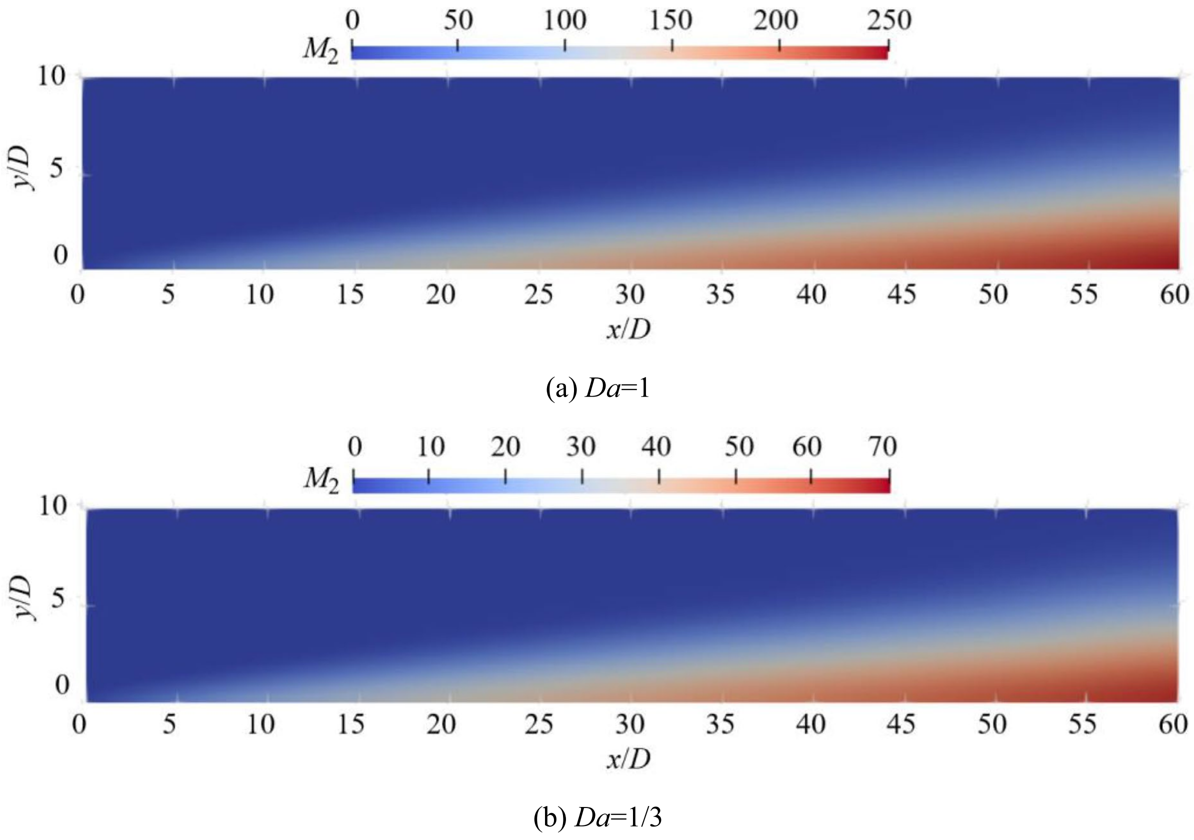

Fig. 9 Distribution of relative particle polydispersity. (**a**) $Da = 1$. (**b**) $Da = 1/3$

Therefore, the values of M_1 decrease slightly along the downstream.

Particle polydispersity

The second-order moment m_2 is proportional to the particle polydispersity. The larger the value of m_2, the wider the particle size distribution. Particle coagulation makes initially monodisperse particles become polydisperse, which can be illustrated by Eq. 24c where the source term on the right-hand side indicates that particle coagulation will increase particle polydispersity and therefore take a positive sign. The relative particle polydispersity is expressed as $M_2 = m_2/m_{20}$ (m_{20} is the initial value of m_2). The distribution of relative particle polydispersity M_2 is shown in Fig. 9 where the values of M_2 increase along the x direction because the further downstream, the more frequent the particles coagulate, resulting in higher polydispersity. However, the values of M_2 are reduced along the y direction due to the small number of particles along the y direction and even the fact that particles are less likely to coagulate. Comparing Fig. 9(a) and (b), the maximum M_2 for $Da = 1$ and $Da = 1/3$ are 250 and 70, respectively, and values of M_2 are larger at $Da = 1$ (a) than that at $Da = 1/3$ (b) in the same region, which indicates that larger Da corresponds to larger value of M_2, i.e., higher polydispersity.

Geometric average diameter of particles

Particle coagulation makes particles change their sizes and results in the difference in particle size

Fig. 10 Distribution of relative geometric average diameter of particles. (**a**) along the *x* direction. (**b**) along the *y* direction

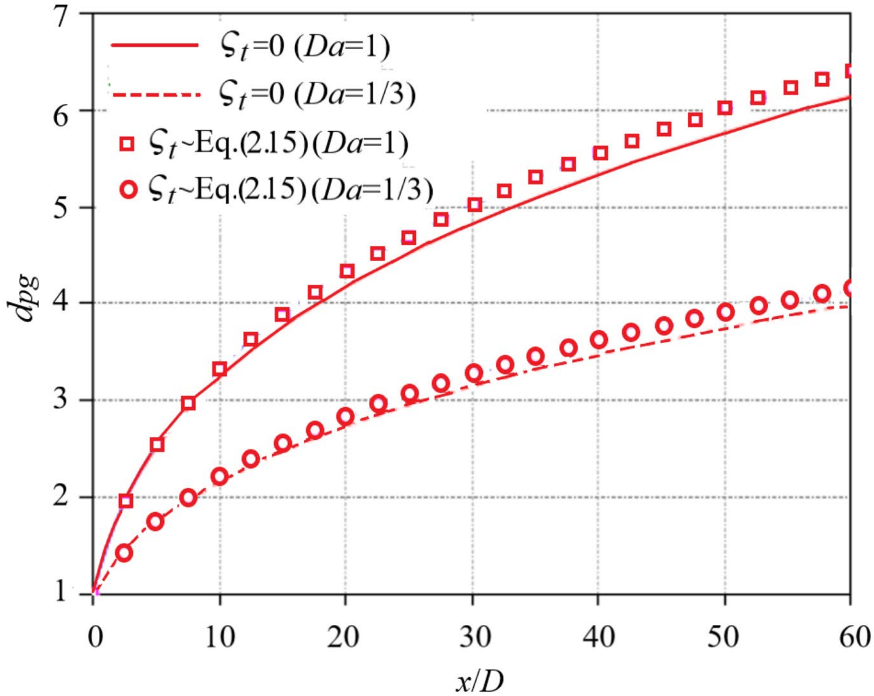

(a) along the *x* direction

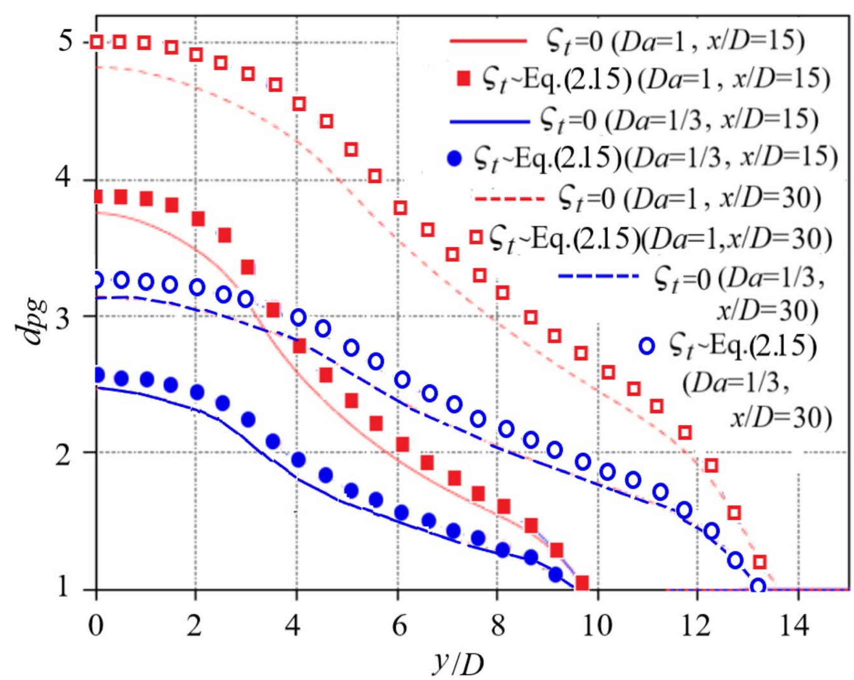

(b) along the *y* direction

Fig. 11 Distribution of relative geometric average diameter of particles. (**a**) along the *x* direction. (**b**) along the *y* direction ($Da = 1$)

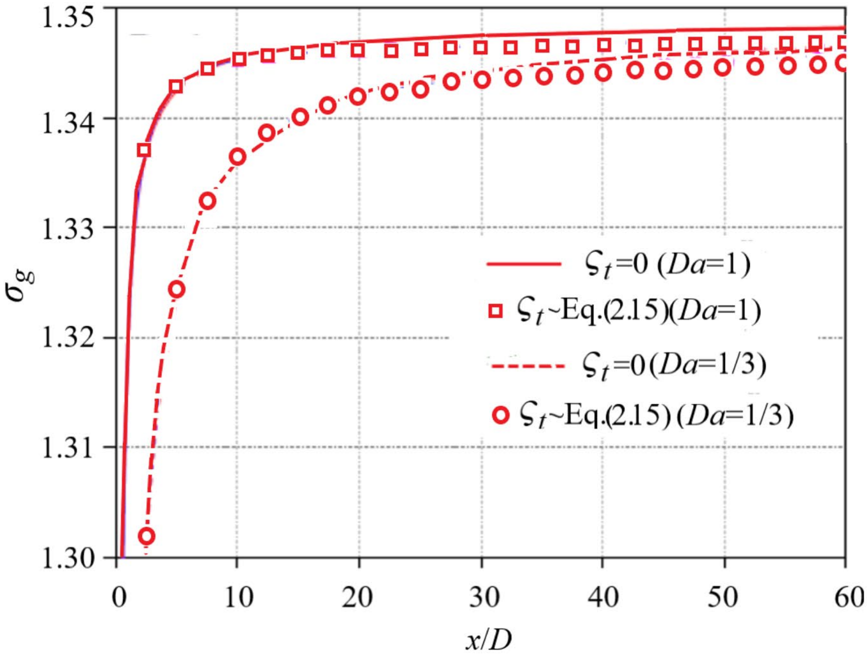

(a) along the *x* direction

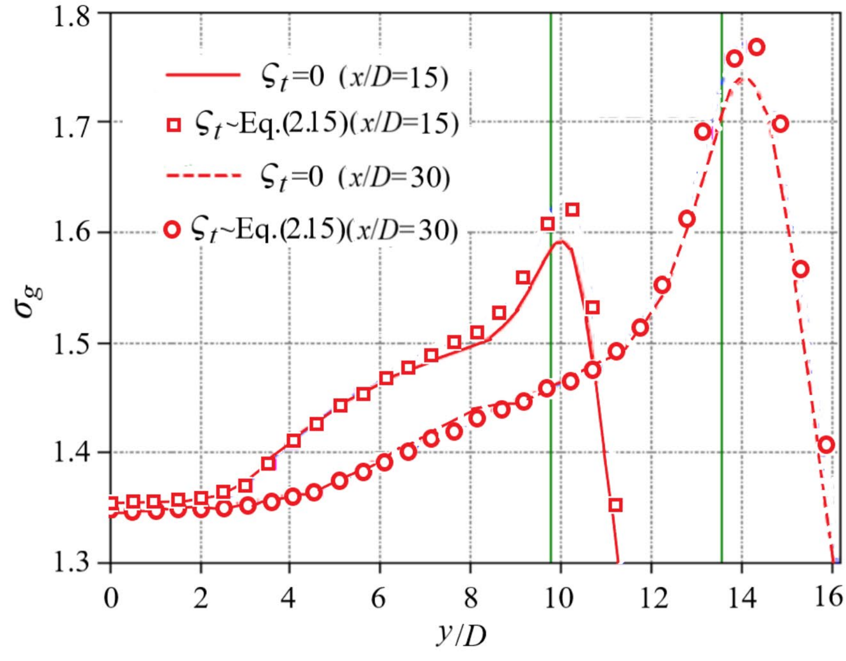

(b) along the *y* direction (Da=1)

which will gradually reach a lognormal distribution and attain self similarity. The relationship between the relative geometric average volume v_g of particles and the first three relative moments is as follows:

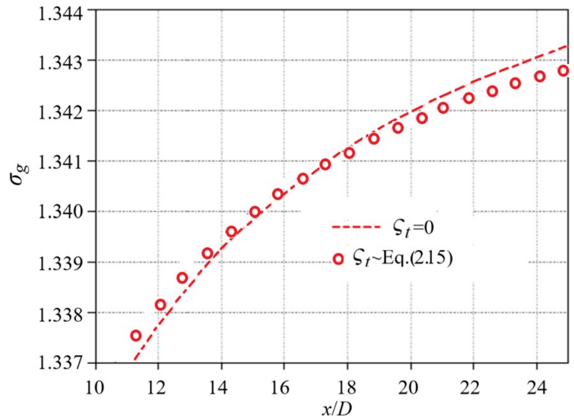

Fig. 12 Locally enlarged view of Fig. 11(a) ($Da = 1/3$)

$$v_g = \frac{M_1^2}{M_0^{3/2} M_2^{1/2}}, \tag{27}$$

and the relative value between the geometric average diameter of particles and their initial diameter is defined as:

$$d_{pg} = v_g^{1/3}. \tag{28}$$

Figure 10 shows the distribution of relative geometric average diameter d_{pg} of particles along the x and y directions. In Fig. 10(a), the values of d_{pg} increase along the x direction because the further downstream, the longer the time of particle coagulation, and the more large particles are formed. At the $x/D = 60$, the value of d_{pg} for $Da = 1$ is 6 times the initial value of d_{pg}, the kernel function of particle coagulation is still applicable because most of the particle sizes still belong to the free molecular region. The growth rate of d_{pg} decreases along the downstream because the low number density of particles downstream leads to the decrease of the coagulation frequency. The larger the value of Da, the faster the particle coagulates, and leading to a larger value of d_{pg} at the same x/D, which can be illustrated by comparing the values of d_{pg} for $Da = 1$ with that for $Da = 1/3$. In the area near the jet inlet ($x/D < 10$), the values of d_{pg} with considering and without considering the fluctuating coagulation are almost the same, but the difference in the value of d_{pg} between both cases gradually increases along the downstream. The maximum relative errors (at $x/D = 60$) reach 5.1% for $Da = 1/3$ and 5.7% for $Da = 1$, respectively.

In Fig. 10(b), the values of d_{pg} decrease from the near-center region to the outer edge of the jet at $x/D = 15$ and 30. This is because the particle number density in the near-center region is high, and the particles coagulate frequently, while the situation at the outer edge of the jet is opposite. In the case of the same Da, the curve shapes at $x/D = 15$ and $x/D = 30$ are very similar, but the values of d_{pg} at $x/D = 30$ are much larger than that at $x/D = 15$. Similarly, in the case of the same x/D, the values of d_{pg} for $Da = 1$ are much larger than that at $Da = 1/3$. The reason has been explained above.

In addition, there is difference in the value of d_{pg} when considering and not considering the fluctuating coagulation. The maximum relative errors (at $x/D = 30$) reach 5.3% for $Da = 1/3$ and 6.4% for $Da = 1$, respectively.

Geometric standard deviation of particle diameter

According to the logarithmic normal distribution function, the relationship between the geometric standard deviation σ_g of particle diameter and the first three moments is:

$$\ln^2 \sigma_g = \frac{1}{9} \ln\left(\frac{M_0 M_2}{M_1^2}\right). \tag{29}$$

For the initial monodisperse particles in the free molecular region, after Brownian coagulation, the particle diameter will reach lognormal distribution of self similarity, and the values of σ_g will gradually reach an asymptotic value $\sigma_{g\infty} = 1.355$ [54, 55]. The distribution of σ_g along the x and y directions is shown in Fig. 11 where the difference in the value of σ_g when considering and not considering the fluctuating coagulation can be seen. The high number density of particles in the area near the jet inlet causes strong coagulation of monodisperse particles, leading to self similarity distribution of particle size in a short period of time. For the case of $Da = 1$ in Fig. 11(a), along the centerline of the jet, the value of σ_g is equal to 1 at $x/D = 0$, and then sharply rises to 1.3 within the range of $0 < x/D < 5$, finally slowly approaches 1.35 (slightly less than the asymptotic value $\sigma_{g\infty} = 1.355$). For the case of $Da = 1/3$, the growth rate of σ_g decreases and its asymptotic value is reduced compared with the case of $Da = 1$. The reason is that small Da means that the diffusion effect of the flow is stronger compared to the coagulation effect, making diameter distribution deviate more from the asymptotic value of the self similar distribution.

In Fig. 11(b), the values of σ_g are very close to 1.35 in the area near the centerline of the jet, but gradually increase in the y direction until the position of the green line. The reason is that, as the distance from the centerline increases, on the one hand, the decrease in particle number density leads to a weakened coagulation effect, which leads to a decrease inσ_g; and on the other hand, the decrease in flow velocity leads to longer time for particles to coagulate, which leads to a increase inσ_g, the combined effect of both leads to an increase in σ_g. In the area where the value of y/D exceeds the green line, the value of σ_g sharply decreases, which is caused by the scarcity of particles in the area. The curve shapes of σ_g at $x/D=15$ and $x/D=30$ are similar, but the span and maximum value of σ_g at $x/D=30$ are much larger than that at $x/D=15$. The maximum relative errors reach 2.5% at $x/D=15$ and 2.9% at $x/D=30$, respectively.

In order to have a clearer understanding of the difference in the value of σ_g when considering and not considering fluctuating coagulation, Fig. 12 shows a locally enlarged view of Fig. 11 at $Da=1/3$. The difference between the two results can be seen.

Conclusion

To illustrate the effect of fluctuating coagulation on particle distribution in multiphase turbulence of nanoparticles, a one-order closed model is proposed to relate the term to the average particle size distribution function. The proposed model and equations are applied to a turbulent jet flow. The main conclusions are summarized as follows.

(1) Numerical results of average velocity and particle volume concentration satisfy self similarity distribution, and numerical results of average velocity, x-component of turbulent kinetic energy, and particle volume concentration are in good agreement with the experimental results, indicating that the presented model, method and program are reliable.

(2) There is a difference in the values of particle number density, geometric average diameter and geometric standard deviation of particle diameter with and without considering fluctuating coagulation, indicating that the fluctuating coagulation cannot be ignored under the flow and parameters in this article.

(3) The larger the value of Da, the faster the particle coagulates, which leads to smaller particle number density, higher particle polydispersity, larger geometric average diameter and geometric standard deviation of particle diameter.

(4) Along the x direction of the flow, particle number density decreases, while particle polydispersity, geometric average diameter, and geometric standard deviation of particle diameter increase because the particles develop downstream, they coagulate more fully. From the centerline to the outer edge of the jet, particle number density, polydispersity and geometric average diameter decrease, while geometric standard deviation of particle diameter increases first and then decreases. The reason is that the decrease in particle number density leads to a weakened coagulation effect, at the same time, the decrease in flow velocity leads to longer time for particles to coagulate, the combined effect of both leads to an increase in geometric standard deviation.

Author contributions **Wenqian Lin**: Methodology (equal); Writing–original draft; Resources. **Hailin Yang**: Methodology (equal); Software. **Jianzhong Lin**: Supervision; review & editing.

Funding This work was supported financially by the National Natural Science Foundation of China (Grant No. 12132015, 12332015).

Data availability The data that support the findings of this study are available from the corresponding author upon reasonable request.

Compliance with ethical standards

Ethics approval and consent to participate No applicable.

Competing interests The authors declare no competing interests.

References

1. Friedlander SK (2000) Smoke, dust and haze: fundamentals of aerosol behavior. Wiley press, New york
2. Saffman PG, Turner JS (1956) On the collision of drops in turbulent clouds. J Fluid Mech 1(1):16–30
3. Delichatsios MA, Probstein RF (1975) Coagulation in turbulent flow: theory and experiment. J Colloid Interface Sci 51(3):394–405
4. Sundaram S, Collins LR (1977) Collision statistics in an isotropic particle-laden turbulent suspension. 1. Direct numerical simulations. J Fluid Mech 335:75–109
5. Wang LP, Wexler AS, Zhou Y (1998) On the collision rate of small particles in isotropic turbulence. I Zero-inertia case Phys Fluids 10(1):266–276
6. Reade WC, Collins LR (2000) A numerical study of the particle size distribution of an aerosol undergoing turbulent coagulation. J Fluid Mech 415:45–64
7. Guichard R, Taniere A, Belut E, Rimbert N (2014) Simulation of nanoparticle coagulation under Brownian motion and turbulence in a differential-algebraic framework: developments and applications. Int J Multiphase Flow 64:73–84
8. Finke J, Niemann S, Richter C, Gothsch T, Kwade A, Buttgenbach S, Muller-Goymann CC (2014) Multiple orifices in customized microsystem high-pressure emulsification: The impact of design and counter pressure on homogenization efficiency. Chem Eng J 248:107–121
9. Chen WC, Cheng WT (2016) Numerical simulation on forced convective heat transfer of titanium dioxide/water nanofluid in the cooling stave of blast furnace. Int Commun Heat Mass Transf 71:208–215
10. Karsch M, Kronenburg A (2023) Modelling nanoparticle agglomeration in the transition regime: A comparison between detailed Langevin Dynamics and population balance calculations. J Aerosol Sci 173:106228
11. Patra P, Roy A (2022) Brownian coagulation of like-charged aerosol particles. Physical Review Fluids 7(6):064308
12. Yang H, Hogan CJ (2017) Collision rate coefficient for charged dust grains in the presence of linear shear. Phys Rev E 96(3):032911
13. Levin LM, Sedunov YS (1966) Gravitational coagulation of charged cloud drops in turbulent flow. Pure Appl Geophys 64(1):185–196
14. Soos M, Marchisio DL, Sefcik J (2013) Assessment of gel formation in colloidal dispersions during mixing in turbulent jets. AIChE J 59(12):4567–4581
15. Cifuentes L, Wlokas I, Wollny P, Kempf A (2023) Turbulence effects on the formation and growth of nano-particles in three-dimensional premixed and non-premixed flames. Appl Energy Combust Sci 16:100210
16. Anand S, Mayya YS (2015) Coagulation in a spatially inhomogeneous plume: Formation of bimodal size distribution. J Aerosol Sci 84:9–13
17. Papini A, Flandoli F, Huang RJ (2023) Turbulence enhancement of coagulation: The role of eddy diffusion in velocity. Physica D-nonlinear Phenomena 448:133726
18. Zhao Y, Kato S, Zhao JN (2016) Numerical investigation of Brownian, gradient, and turbulent coagulation under moving vehicle conditions in an underground garage. J Disper Sci Technol 372(2):258–269
19. Zatevakhin MA, Ignatyev AA, Govorkova VA (2015) Numerical simulation of Brownian coagulation under turbulent mixing conditions. IZV Atmos Ccean Phy 51(2):148–155

20 Chan TL, Liu SY, Yue Y (2018) Nanoparticle formation and growth in turbulent flows using the bimodal TEMOM. Powder Technol 323:507–517

21. Settumba N, Garrick SC (2003) Direct numerical simulation of nanoparticle coagulation in a temporal mixing layer via a moment method. J Aerosol Sci 34(2):149–167
22. Miller SE, Garrick SC (2004) Nanoparticle coagulation in a planar jet. Aerosol Sci Technol 38(1):79–89
23. Garrick SC, Lehtinen KEJ, Zachariah MR (2006) Nanoparticle coagulation via a Navier–Stokes/Nodal methodology: evolution of the particle field. J Aerosol Sci 37(5):555–576
24. Garrick SC (2011) Effects of turbulent fluctuations on nanoparticle coagulation in shear flows. Aerosol Sci Technol 45(10):1272–1285
25. Ma HY, Yu MZ, Jin HH (2020) A study of the evolution of nanoparticle dynamics in a homogeneous isotropic turbulence flow via a DNS-TEMOM method. J Hydrodyn 32(6):1091–1099
26. Cifuentes L, Sellmann J, Wlokas I, Kempf A (2020) Direct numerical simulations of nanoparticle formation in premixed and non-premixed flame-vortex interactions. Phys Fluids 32(9):093605
27. Schwarzer HC, Schwertfirm F, Manhart M, Schmid HJ, Peukert W (2006) Predictive simulation of nanoparticle precipitation based on the population balance equation. Chem Eng Sci 61(1):167–181
28. Das S, Garrick SC (2010) The effects of turbulence on nanoparticle growth in turbulent reacting jets. Phys Fluids 22(10):103303
29. Rigopoulos S (2007) PDF method for population balance in turbulent reactive flow. Chem Eng Sci 62(23):6865–6878
30. Warshaw M (1967) Cloud droplet coalescence: statistical foundations and a one-dimensional sedimentation model. J Atmos Sci 24(3):278–286
31. Levin LM, Sedunov YS (1968) The theoretical model of the drop spectrum formation process in clouds. Pure Appl Geophys 69(1):320–335
32. Loeffler J, Das S, Garrick SC (2011) Large eddy simulation of titanium dioxide nanoparticle formation and growth in turbulent jets. Aerosol Sci Technol 45(5):616–628
33. Tsagkaridis M, Rigopoulos S, Papadakis G (2022) Analysis of turbulent coagulation in a jet with discretised population balance and DNS. J Fluid Mech 937:A25
34. Drossinos Y, Housiadas C (2006) Aerosol flows. In Multiphase Flow Handbook (ed. C.T. Crowe), 6–1–6–58. CRC Press
35. Spalding DB (1971) Concentration fluctuations in a round turbulent free jet. Chem Eng Sci 26(1):95–107
36. Elghobashi S, Pun W, Spalding D (1977) Concentration fluctuations in isothermal turbulent confined coaxial jets. Chem Eng Sci 32(2):161–166

37. Yang H (2023). On the hydrodynamics and heat transfer characteristics of nanoparticle multiphase flow. Doctoral Dissertation, Zhejiang University, China
38. Pratsinis SE (1988) Simultaneous nucleation, condensation and coagulation in aerosol reactors. J Colloid Interface Sci 124:416–427
39. Marchisio DL, Fox RO (2005) Solution of population balance equations using the direct quadrature method of moments. J Aerosol Sci 36:43–73
40. Barrett JC, Jheeta JS (1996) Improving the accuracy of the moments method for solving the aerosol general dynamic equation. J Aerosol Sci 27:1135–1142
41. Frenklach M (2002) Method of moments with interpolative closure. Chem Eng Sci 57:2229–2239
42. Yu MZ, Lin JZ, Chan TL (2008) A new moment method for solving the coagulation equation for particles in Brownian motion. Aerosol Sci Technol 42:705–713
43. Yu MZ, Lin JZ (2010) Binary homogeneous nucleation and growth of water-sulfuric acid nanoparticles using a TEMOM model. Int J Heat Mass Tran 53(4):635–644
44. Yu MZ, Lin JZ, Jin HH, Jiang Y (2011) The verification of the Taylor-expansion moment method for the nanoparticle coagulation in the entire size regime due to Brownian motion. J Nanopart Res 13(5):2007–2020
45. Yu MZ, Liu YY, Lin JZ, Seipenbusch M (2015) Generalized TEMOM scheme for solving the population balance equation. Aerosol Sci Technol 49:1021–1036
46. Xie ML, Wang LP (2013) Asymptotic solution of population balance equation based on TEMOM model. Chem Eng Sci 94:79–83
47. Klein M, Sadiki A, Janicka J (2003) Investigation of the influence of the Reynolds number on a plane jet using direct numerical simulation. Int J Heat Fluid Flow 24(6):785–794
48. Ribault C, Le Sarkar S, Stanley SAS (1999) Large eddy simulation of a plane jet. Phys Fluids 11(10):3069–3083
49. Gutmark E, Wygnanski I (1976) Planar turbulent jet. J Fluid Mech 73(10):465–495
50. Ramaprian B, Chandrasekhara M (1985) LDA measurements in plane turbulent jets. J Fluid Eng-T ASME 107(2):264–271
51. Davies A, Keffer J, Baines W (1975) Spread of a heated plane turbulent jet. Phys Fluids 18(7):770–775
52. Jenkins P, Goldschm VW (1973) Mean temperature and velocity in a plane turbulent jet. J Fluid Eng-T ASME 95(4):581–584
53. Heskesta G (1965) Hot-wire measurements in a plane turbulent jet. Int J Appl Mech 32(4):721–734
54. Lee K, Chen H, Gieseke J (1984) Log-normally preserving size distribution for Brownian coagulation in the free-molecule regime. Aerosol Sci Technol 3(1):53–62
55. Chen Z, Lin JZ, Yu MZ (2013) Asymptotic behavior of the Taylor-expansion method of moments for solving a coagulation equation for Brownian particles. Particuology 14:124–129